Advances in Materials Research, *Vol. 4, No. 4 (2015) 193-205*
DOI: http://dx.doi.org/10.12989/amr.2015.4.4.193

Characterizations of nano-zinc doped hydroxyapatite to use as bone tissue engineering

Basma E. Abdel-Ghany[1], Bothaina M. Abdel-Hady[1], Abeer M. El-Kady[1a], Hanan H. Beheiry[1] and Osiris W. Guirguis[*2]

[1]*Biomaterials Department, Advanced Materials and Nanotechnology Lab, National Research Centre, Giza, Egypt*
[2]*Biophysics Department, Faculty of Science, Cairo University, Giza, Egypt*

(Received July 4, 2015, Revised December 8, 2015, Accepted December 10, 2015)

Abstract. Contamination by bacterial strands is a major problem after bone replacement surgeries, so there is a great need to develop low cost biocompatible antibacterial bioactive scaffolds to be used in bone tissue engineering. For this purpose, nano-zinc doped hydroxyapatite with different zinc-concentrations (5, 10 and 15 mol%) was successfully prepared by the wet chemical precipitation method. The prepared powders were used to form porous scaffolds containing biodegradable Ca-cross-linked alginate (5%) in order to enhance the properties of alginate scaffolds. The scaffolds were prepared using the freeze-gelation method. The prepared powders were tested by X-ray diffraction; transmission electron microscope and Fourier transform infrared analyses, while the prepared scaffolds were investigated by Fourier transform infrared analyses, thermogravimetric analyses and measurement of the antibacterial properties. Best results were obtained from scaffold containing 15% mol zinc-doped hydroxyapatite powders and 5% alginate concentration with ratio of 70:30.

Keywords: bioceramics; nano-zinc doped hydroxyapatite; scaffolds; nanostructure; antimicrobial activity

1. Introduction

Bone is a dynamic tissue which undergoes remodeling, as it is constantly being resorbed and rebuilt (or formed), following injury (Rho *et al.* 1998). However, many circumstances call for bone grafting owing to bone defects, either from traumatic or from non-traumatic destruction. The currently used alternatives, such as mechanical devices or artificial prostheses do not repair the tissue or organ function and are not intended to integrate into the host tissue (Maguire *et al.* 1987)**.**

In such situations, bone tissue engineering can bring up the ultimate solution and hope for many patients suffering from these problems. The purpose of tissue engineering is achieved using biomimetic bioactive degradable biomaterials to either induce surrounding tissue and cell ingrowth or to serve as temporary scaffold for transplanted cells to attach, grow, and maintain differentiated

*Corresponding authors, Ph.D., E-mail: osiris_wgr@yahoo.com
[a]Ph.D., E-mail: abeerelkady_2000@yahoo.co.uk

http://www.techno-press.org/?journal=amr&subpage=7 ISSN: 2234-0912 (Print), 2234-179X (Online)

functions leaving only natural substances to restore normal organ function (Tateishi *et al.* 2002). One of the most important stages of bone tissue engineering (TE) is the design and processing of a porous, biodegradable three-dimensional structure called a 'scaffold', exhibiting high porosity, high pores interconnectivity and uniform pores distribution (Mourinõ and Boccaccini 2010, Ninan *et al.* 2013, Sowjanya *et al.* 2013, Xia *et al.* 2013). These scaffolds should provide structural support for cells and the new tissue being formed, acting as a temporary extracellular matrix inducing the natural processes of tissue regeneration and development.

Natural polymers as alginate have been focused on with more attention to be used in tissue engineering applications, because of their biocompatibility and biodegradability. Calcium phosphates especially hydroxyapatite have been focused on owing to their chemical and structural similarity with natural bone mineral. On the other hand, hydroxyapatite is brittle and has shaping difficulty. In order to enhance the properties of alginate, calcium phosphates were used to enhance its bioactivity and mechanical properties. Recent studies (Chen *et al.* 2012, Sutha *et al.* 2013) have focused on the development of antibacterial scaffolds to prevent risky infections from surgeries. For this purpose zinc-substituted hydroxyapatite is used.

The present study was designed to study the effect of zinc substitution on hydroxyapatite properties. Establish the feasibility of synthesis of biodegradable bioactive antibacterial Al/Zn-HA 3D scaffolds of different zinc concentrations by applying freeze-gelation method with structural homogeneity. Zinc-doped hydroxyapatite nanoparticles were chosen as fillers to induce the antibacterial properties to the prepared scaffolds with gain of more insight into the microstructure and physicochemical properties of the fabricated scaffolds. Therefore, the aim of the present work is to prepare easily shaped antibacterial scaffolds from zinc-substituted hydroxyapatite and alginate by using the wet chemical precipitation method and freeze-gelation method to be used for bone tissue engineering surgeries. The antibacterial test to choose the best zinc concentration in reducing the bacterial counts after immersion in *Staphylococcus aureus* broth for 24 h was also studied.

2. Materials and methods

Hydroxyapatite, 5, 10 and 15 mol% zinc substituted hydroxyapatite powders were initially prepared by the wet chemical precipitation method using $Ca(NO_3)_2$, $(NH_4)_2HPO_4$, and $Zn(NO_3)_2$ aqueous solutions as reagents (Miyaji *et al.* 2005). The resulting powders were dried at 100 ^oC over night and were used as prepared for the scaffolds preparation. The samples were coded as, HA, 5% Zn-HA, 10% Zn-HA and 15% Zn-HA, respectively.

Phase analyses of the as prepared powders were studied using X-ray powder diffractometer (XRD), Brukur D8 Advanced Cu target with secondary monochromator) operated at 40 kV and 40 mA. Morphology and nano size assurance of the as prepared powders were examined via transmission electron microscope (TEM, Jeol JEM 1230) operated at 120 kV. The functional groups present in the prepared powders were assured by Fourier transform infrared spectrophotometer (FTIR/6100 type A). The FTIR spectra were obtained over the region 4000-400 cm^{-1} using KBr pellet transmission technique with a resolution of 4 cm^{-1}.

The as prepared HA, 5% Zn-HA, 10% Zn-HA and 15% Zn-HA powders were processed into a 3D scaffold (5 wt%) using the freeze-gelation method (Ho *et al.* 2004). The ratio of as prepared powders to alginate was kept constant (70:30). The prepared scaffolds were given the codes HA/Alg, 5% Zn-HA/Alg, 10% Zn-HA/Alg and 15% Zn-HA/Alg, respectively. In addition, neat

alginate scaffold (Alg) was prepared for comparison. The scaffolds were characterized by FTIR. Thermal stability and weight loss of the prepared powders and scaffolds were observed as a function of temperature by thermogravimetric instrument (TGA, Perkin Elmer-TGA 7). The test was performed from room temperature (about 20°C) up to 1000 ^{o}C under N_2-atmosphere with heating rate was 10°C/minute. The surface of the prepared scaffolds was investigated using scanning electron microscope (SEM, Jeol JXA 840). The samples were sputtered with gold by a sputter coater as an adhesive and electronic conductor. Finally, the antibacterial properties of the prepared scaffolds were evaluated based on the colony count method. The liquid state tests can indicate the interaction of different antibacterial scaffolds with bacteria and show whether the release of Zn ions into the medium can be harmful to the gram-positive *Staphylococcus aureus* (Chung *et al.* 2005). *S. aureus* is used after being thawed from the freezer and transferred into Brain Heart Infusion Broth (BHI), incubated at 37°C for 24 h. After observing sufficient growth observation, the culture was diluted in saline solution to appropriate target inocula. In order to prevent contamination from other biological species, scaffolds, applied in the anti-microbial tests, were soaked in ethanol for 10 minutes. All tests were performed under sterile conditions in duplicates and repeated three times.

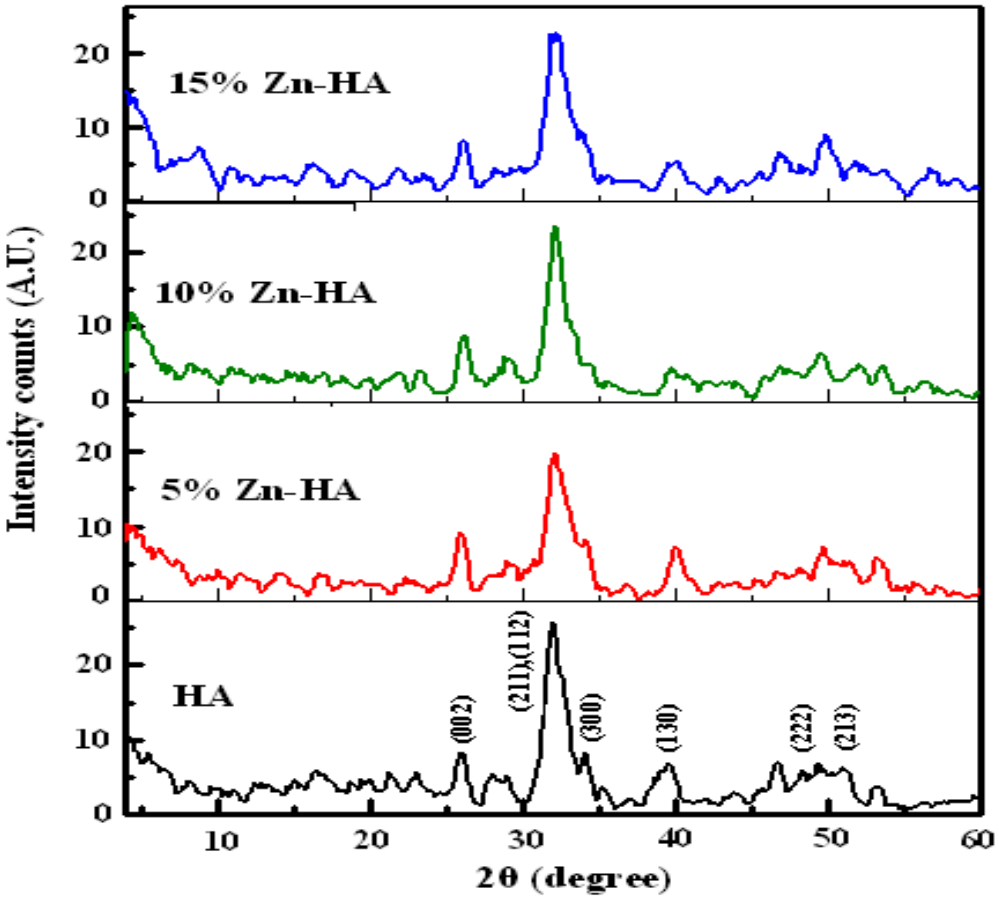

Fig. 1 X-ray diffraction patterns of the prepared powders

Table 1 Changes in HA properties with increasing zinc fraction

Sample code	FWHM		Single crystal dimension of HA and Zn-HA (nm)		Unit cell volume ($Å^3$)	Crystallinity (X_c)
	a-axis (300)	*c*-axis (002)	*a*-axis (300)	*c*-axis (002)		
HA	0.72	0.41	23.02	39.99	18.35	0.202
5% Zn-HA	0.68	0.58	24.38	27.80	14.31	0.068
10% Zn-HA	0.90	0.59	18.28	27.67	8.60	0.067
15% Zn-HA	0.96	0.60	17.25	27.21	7.01	0.064

3. Results and discussion

3.1 Powder characterization

The XRD patterns of the prepared HA, 5% Zn-HA, 10% Zn-HA and 15% Zn-HA powders are shown in Fig. 1. It is clear from the figure that, the observed pattern of HA sample indicates several distinct crystalline peaks at 2θ= 25.79, 31.68, 33.68, 38.95, 47.58 and 50.42 degrees, assigned to (002), (211,112), (300), (130), (222) and (213), respectively, assigned to the apatite structure and matches the ICDD standard for HA (JCPDS No. 76-0694). These diffraction peaks become wider and less intense as the Zn fraction increases which could be due to: (1) the ionic radius is smaller in Zn^{2+} (0.074 nm) than in Ca^{2+} (0.099 nm); (2) the effect of zinc addition on the lattices parameters and crystal size or (3) the significant decrease of apatite crystallinity due to zinc addition (Li *et al.* 2008, Ren *et al.* 2009, Suresh Kumar *et al.* 2012).

As noticed from Table 1 that, the lattice parameter (a) increased with increasing Zn fraction up to 5 mol% and decreased over 5 mol% Zn. On the other hand, the lattice parameter (c) decreased with increasing Zn fraction and became nearly constant over 5 mol% Zn. Such contraction in the lattice parameters (a) and (c) may reflect the difference in the atomic radius between Ca and Zn atoms, which in turn must influences the crystal structure of the HA and induces a reduction in the crystallite size (Li *et al.* 2008, Ren *et al.* 2009, Suresh Kumar *et al.* 2012). As shown from Table 1, the single-crystal dimensions of all the prepared powders were less than 40 nm.

Crystallinity is defined as the weight fraction of the crystalline portion. The physical and mechanical properties of material are considerably dependent on that parameter. XRD is used to measure the crystallinity. The crystallinity index (CrI) was calculated for the prepared samples using the relation (Segal *et al.* 1959)

$$CrI = [(I_f - I_s)/I_f] \times 100 \quad (1)$$

Where I_f is the peak intensity of the fundamental band at 2θ=31.68° and I_s is the peak intensity of the secondary band at 2θ=25.79°. The CrI represents a time-save empirical measure of relative crystallinity. Table 2 illustrates the variation of crystallinity index (CrI) and their percentage change of the prepared HA, 5% Zn-HA, 10% Zn-HA and 15% Zn-HA powders calculated from the X-ray patterns (Fig. 1). It is clear from the table that, the values of CrI of the samples decreases with Zn concentration. This implies changes in the structural of hydroxyapatite with increasing zinc fraction.

Table 2 Variations in the crystallinity index (CrI) of the prepared HA, 5% Zn-HA, 10% Zn-HA and 15% Zn-HA powders

Sample code	Crystallinity index (CrI)	Δ(CrI)% *
HA	66.95	-
5% Zn-HA	52.78	21.2
10% Zn-HA	61.14	8.7
15% Zn-HA	61.88	7.6

$$^{*}\Delta(\mathrm{CrI})\% = \frac{(\mathrm{CrI})_{HA} - (\mathrm{CrI})_{Zn\text{-}HA}}{(\mathrm{CrI})_{HA}} \times 100$$

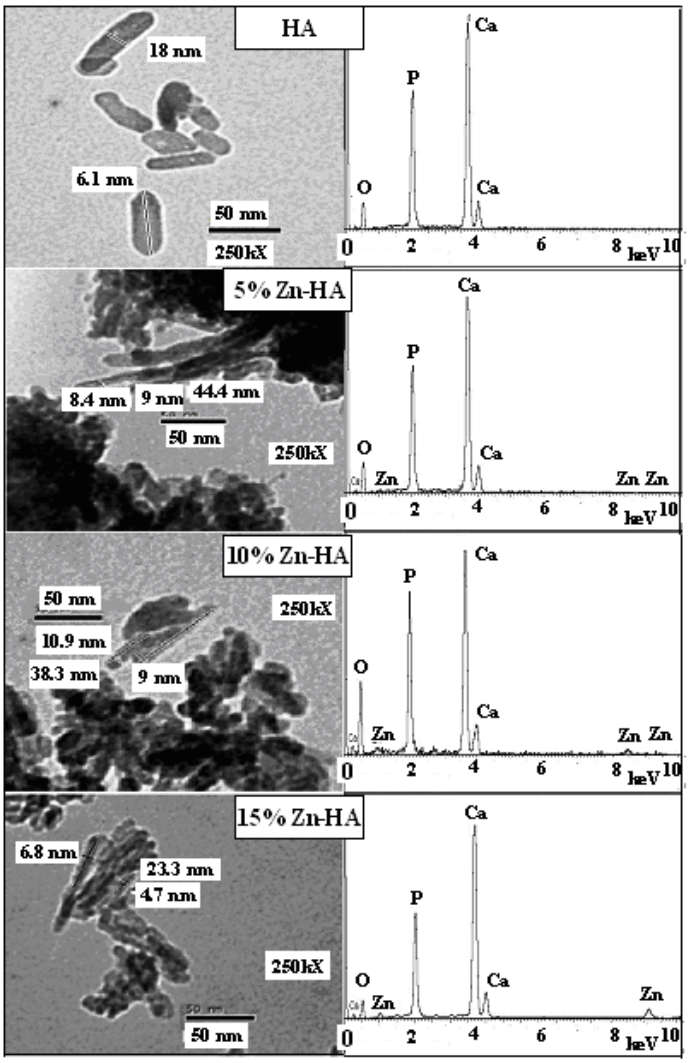

Fig. 2 TEM at a magnification of 250 kX and EDX of the prepared powders

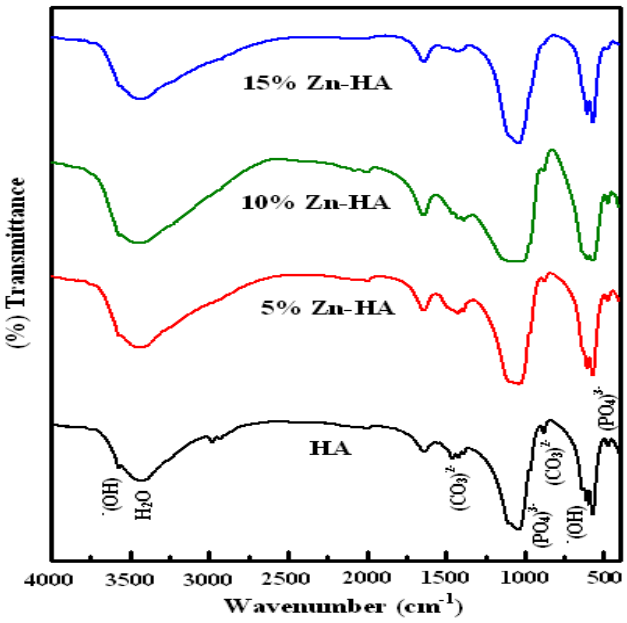

Fig. 3 FTIR spectra of the prepared powders

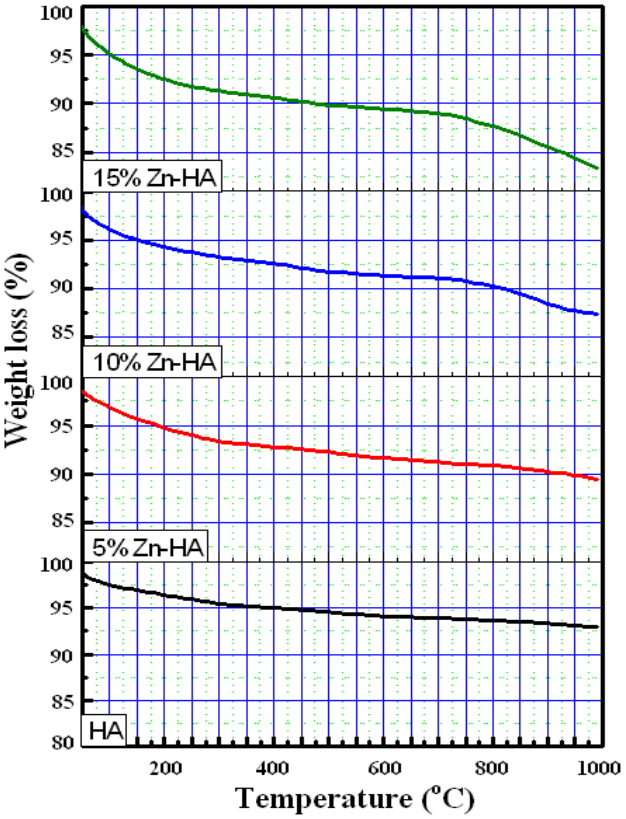

Fig. 4 TGA curves for the prepared powders

The TEM micrographs of the prepared HA, 5% Zn-HA, 10% Zn-HA and 15% Zn-HA powders were shown in Fig. 2. The figure includes their EDX spectra, which indicate the incorporation of zinc into the structures of 5, 10 and 15% Zn-HA. Examining the TEM micrographs revealed that, the increase of zinc fraction has a negative effect on the crystal size, the mean value size decreases with increasing zinc fraction. From the figure, it was shown that the pure HA is in the form of stick-shaped crystallites, however, more needle-shaped crystallites increase with increasing zinc fraction, which agrees with the previously reported results (Li *et al.* 2008). From the picture, aggregates consisting of interconnected rod-like particles with about 40-60 nm in length and 4-12 nm in width were observed. The size of the apatite particles was reduced with increasing zinc fraction, which agrees with the XRD data. In the human body, the crystal size of apatite particle is about (5-20)×60 nm (Li *et al.* 2008). Therefore, to a certain extent the size of the prepared powders prepared by the wet chemical precipitation matches with the natural HA.

FTIR spectra of the prepared HA, 5% Zn-HA, 10% Zn-HA and 15% Zn-HA powders were shown in Fig. 3. It is clear from the figure that, with increasing zinc fraction, the separation of the three PO_4^{3-} stretching bands become obscure (Miyaji *et al.* 2005) and the $^-$OH bending peak at 631 cm^{-1} broadens. These changes suggest that the crystallinity of the apatite decreases as the zinc fraction increases, which is matching with the results of the XRD patterns (Li *et al.* 2008).

TGA curves of the prepared HA, 5, 10 and 15% Zn-HA are shown in Fig. 4. All curves show the vaporization of apatite lattice H_2O that might gradually occur at 140-600 °C nearly 7% and a second decomposition at nearly 750°C due to the decarbonation of HA and decomposition of the apatite to form TCP ($Ca_3(PO_4)_2$). The weight loss increases with the increase of zinc concentration from 7 to 16% through the whole temperature up to 1000°C which might be related to Zn promotion for the transformation of apatite to TCP (Miyaji *et al.* 2005, Li *et al.* 2008, Ren *et al.* 2009, Suresh Kumar *et al.* 2012). It was noticed from the thermal analysis that the prepared powders are thermally stable to a relative extent, but this thermal stability decreases with increasing zinc fraction due to crystal deformation caused by zinc substitution, which may promote apatite transformation to TCP.

3.2 Scaffold characterization

FTIR spectra of the prepared Alg, HA/Alg, 5% Zn-HA/Alg, 10% Zn-HA/Alg and 15%-HA/Alg scaffolds with hydroxyapatite to alginate ratio of 70:30 and alginate concentration of 5% were shown in Fig. 5. The FTIR spectrum of alginate scaffold shows the following bands (Ribeiro *et al.* 2004): 3422 cm^{-1} corresponds to $^-$OH stretching, 2926 cm^{-1} corresponds to C-H stretching. 1617 cm^{-1} corresponds to COO^- asymmetrical stretching, 1428 cm^{-1} COO^- symmetrical stretching. 1320 cm^{-1} corresponds to C-O stretching, 1089 cm^{-1} band corresponds to COH stretching. 1036 cm^{-1} corresponds to τ(CO), δ(CCO), δ(CC) vibrational modes. 948 cm^{-1} corresponds to ν(CO), δ(CCH) vibrational modes, 890 cm^{-1} corresponds to ν(CO), δ(CCH) vibrational modes and the peak at 817 cm^{-1} identified as a combination of three possible vibrational modes ($\tau_{CO}+\delta_{CCO}+\delta_{CCH}$). For HA/Alg and Zn-HA/Alg scaffolds a new strong absorption band can be observed at 552 cm^{-1} which is attributed to the bending of PO_4^{3-} of HA (Zhang *et al.* 2003). According to Ma *et al.* (2006), HA should have an absorption band at 1035 cm^{-1} due to the stretching of PO_4^{3-}. However, it was well known that alginate also has a strong absorption band at this position **(**Jin *et al.* 2008).

Thus, the observed broad band at 1032 cm^{-1} is attributed to the overlap of C-O-C stretching of alginate and PO_4^{3-} stretching of HA. The broad band at 3446 cm^{-1} in the spectrum of HA/Alg is assigned to stretching of the $^-$OH groups of alginate, HA and absorbed water. There is nearly no

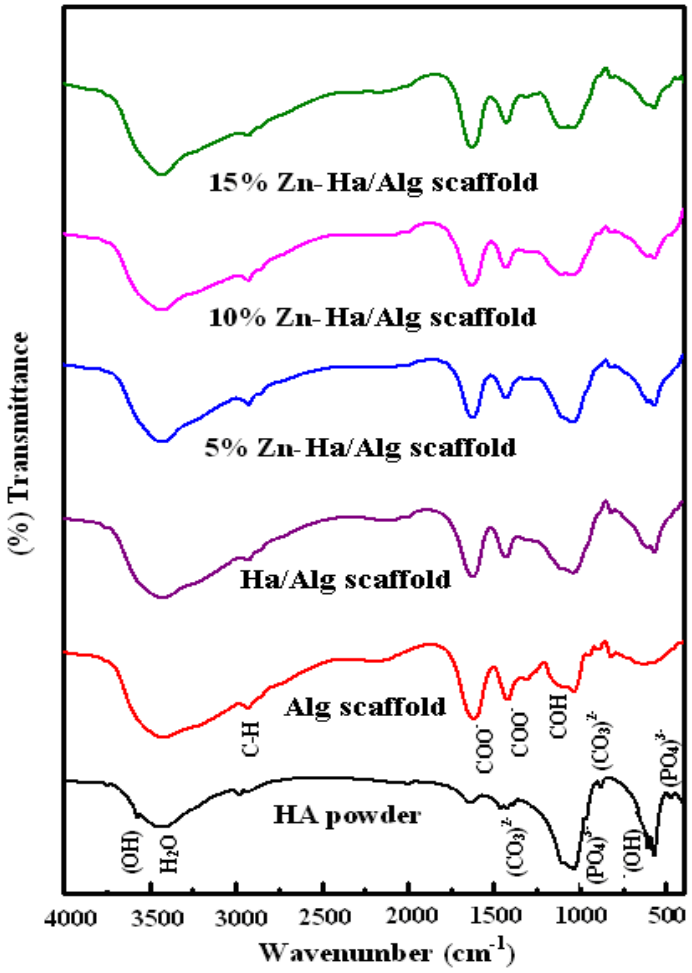

Fig. 5 FTIR spectra of the prepared scaffolds

effect of increasing zinc concentration due to the masking effect of alginate absorbance peaks.

TGA curves for the prepared scaffolds HA/Al, 5% Zn-HA/Alg, 10% Zn-HA/Alg and 15% Zn-HA/Alg with hydroxyapatite to alginate ratio of 70:30 and alginate concentration of 5% is shown in Fig. 6. The prepared scaffolds show a decomposition at about 60^{o}C with loss of water and alginate decomposition by about 10%. A second decomposition at a range of temperature 106-190^{o}C due to a progressive rupture of alginate and the dehydration and condensation of HPO_4^{2-} group as well as vaporization of HA lattice H_2O that might gradually occur at the range 140-600 ^{o}C by about 20%.

As the concentration of zinc increases, a third decomposition appears at about 800^{o}C which may be due to the decarbonation of HA and decomposition of the apatite to form TCP [$Ca_3(PO_4)_2$] and also decomposition of alginate residues. The weight loss fairly increases with the increase of zinc concentration from 2.4 to 8% which might be referred to zinc promotion for the transformation of apatite to TCP (Miyaji *et al.* 2005, Li *et al.* 2008, Ren *et al.* 2009, Suresh Kumar *et al.* 2012).The results confirm that the HA:Alg ratio is 70:30.

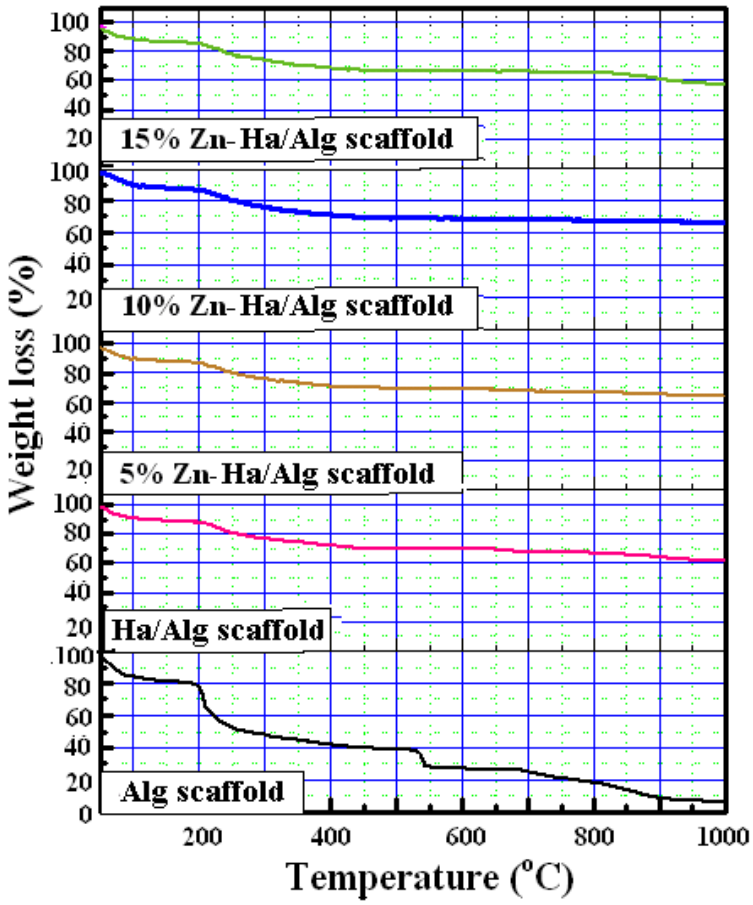

Fig. 6 TGA curves for the prepared scaffolds

Morphology of Alg, 5% Zn-HA/Alg and 15% Al/Zn-HA/Alg scaffolds was investigated using scanning electron microscope (SEM) is shown in Fig. 7. All scaffolds exhibited porous structure with interconnected continuous pores ranging in the size from about 6 to 440 μm. Pore size is calculated by the instrument's software, so the maximum and the minimum pore size were detected. The maximum detected pore size of the prepared Alg, 5% Zn-HA/Alg and 15% Al/Zn-HA/Alg scaffolds are about: 440, 416 and 336 μm, respectively. The minimum detected pore size of the prepared Alg, 5% Zn-HA/Alg and 15% Al/Zn-HA/Alg scaffolds are about: 47, 24 and 6 μm, respectively.

Many authors reported that a maximal tissue in growth is attained with a pore size ranging from 200 to 400 μm (Lu and Mikos 1996), for others it should be from 100 to 150 μm (Maquet and Jerome 1997), or from 100 to 350 μm (Whang *et al.* 1998), for example. Interconnectivity between pores is highly desirable when compared to the isolated pores, since an interconnected pore network structure enhances the diffusion rates to and from the centre of the scaffold and facilitates vascularization, thus improving oxygen and nutrient supply and waste removal. In general, scaffold should have different pore sizes to allow cell penetration; < 50 μm pores sufficient to ingrowth of fibrous tissue; > 100 μm pores needed for new bone generation; and > 200 μm pores

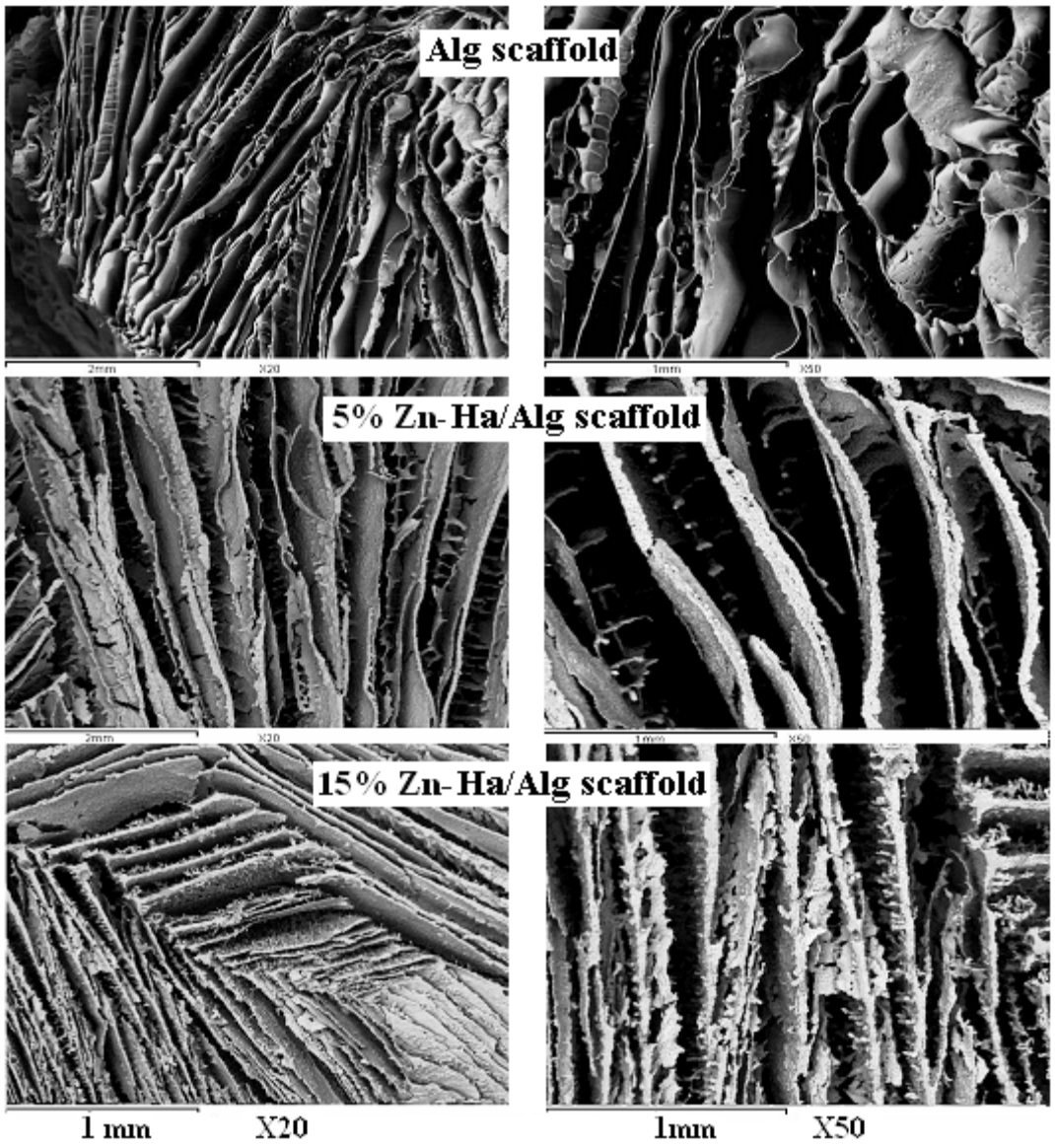

Fig. 7 SEM at two different magnifications of 5% Al, 5% Al/Zn-HA and 15% Al/Zn-HA scaffolds

required for mature osteons to be formed. All pore size ranges are present in the present prepared scaffolds as illustrated in the figure. The combination of the axial orientation and the micro-porosity may therefore simultaneously promote cell attachment and revascularization within the scaffold. The alginate chains appear to be orderly mineralized with HA nanoparticles that cover the flat area of the polymeric ribbons which are organized in a network. As shown in Fig. 7, alginate causes the formation of a typical egg-box structure which is the result of anisotropic growth of isomorphological molecular units (Cho *et al.* 2005, Xu *et al.* 2005). The rigid egg-box association allows a more opened pore structure of alginate with high porosity. The interaction of

nano Zn-HA and alginate makes some G-blocks incapable of forming an egg-box model leading into more closed pores, smaller pore sizes and thicker walls (Xu *et al.* 2005). Thus, the interaction of nano Zn-HA with alginate results in less porous and more closed structures, pore size decreases with increasing Zn-HA content.

The average CFU/mL counts with corresponding standard deviations in duplicates and within 3 replicates of *Staphylococcus aureus* after 24 h in both 15 and 50 mL broth were listed in Table 3 and expressed.

Table 3 Average and standard deviation of the logarithm of colony-forming units per milliliter (CFU/ mL) of *Staphylococcus aureus* after 24 h

Sample code	15 mL broth		50 mL broth	
	Log (10) CFU/mL	P-value**	Log (10) CFU/mL	P-value**
Control*	10.250 ± 0.178	-	10.250 ± 0.178	-
Alg scaffold	10.477 ± 0.221	> 0.05	10.582 ± 0.223	> 0.05
HA scaffold	9.959 ± 0.284	> 0.05	10.097 ± 0.149	> 0.05
5% Zn-HA/Alg scaffold	7.591 ± 0.259	> 0.0001	9.477 ± 0.254	< 0.01
10% Zn-HA/Alg scaffold	6.079 ± 0.206	> 0.0001	8.491 ± 0.172	> 0.0001
15% Zn-HA/Alg scaffold	4.602 ± 0.255	> 0.0001	6.903 ± 0.327	> 0.0001

*Control: broth containing no scaffolds.
***P*>0.05, the difference is not significant (NS), *P*<0.01, the difference is significant (S), and *P*<0.0001, the difference is very high significant (VHS).

From the table, it is clear that after incubating the scaffolds at 37°C for 24 h in broth medium, alginate scaffolds show slightly higher counts than control, which may be due to the nature of alginate as a polysaccharide, which may act as a bacterial nutrient. HA scaffolds show moderate antibacterial effect which agrees with previously reported results obtained (Tin-Oo *et al.* 2007). As the zinc fraction increases, there is a decrease in the bacterial count, which was attributed to zinc ions release. Since these zinc ions have well documented antibacterial properties (Chen *et al.* 2012, Sutha *et al.* 2013), the solution become clearer with increasing the zinc content. So, Zn-HA/Alg scaffold can use as an antibacterial scaffold. From the antibacterial test and Table 3, it was illustrated that the best zinc concentration in reducing the bacterial counts after immersion in *S. aureus* broth for 24 h is the 15% zinc hydroxyapatite/alginate scaffold.

4. Conclusions

Zinc-doped hydroxyapatite nanoparticles with different zinc concentrations (5, 10 and 15 mol%) were successfully prepared and characterized. Also, 3D scaffolds were prepared by blending the powders with alginate polymer (5 wt%) using the freeze-gelation method. The prepared scaffolds were characterized by FTIR, TGA, and SEM as well as by measuring their antibacterial properties. Best results were obtained from scaffolds containing 15 mol% zinc-doped hydroxyapatite powder and 5% alginate concentration with a ratio of 70:30.

Acknowledgements

This work was carried out through the collaboration between Biomaterials Department, National Research Center (NRC) and Biophysics Department, Faculty of Science, Cairo University, Egypt.

References

Chen, X., Tang, Q.L., Zhu, Y.J., Zhu, C.I. and Feng, X.P. (2012), "Synthesis and antibacterial property of zinc loaded hydroxyapatite nanorods", *Mater. Lett.*, **89**, 233-235.

Cho, S.H., Oh, S.H. and Lee, J.H. (2005), "Fabrication and characterization of porous alginate/polyvinyl alcohol hybrid scaffolds for 3D cell culture", *J. Biomater. Sci., Polym. Ed.*, **16**(8), 933-947.

Chung, R.J., Hsieh, M.F., Huang, K.C., Perng, L.H., Chou, F.I. and Chin, T.S. (2005), "Anti-microbial hydroxyapatite particles synthesized by a sol-gel route", *J. Sol-gel Sci. Tech.*, **33**(2), 229-239.

Ho, M.H., Kuo, P.Y., Hsieh, H.J., Hsien, T.Y., Hou, L.T., Lai, J.Y. and Wang, D.M. (2004), "Preparation of porous scaffolds by using freeze-extraction and freeze-gelation methods", *Biomater.*, **25**(1), 129-138.

Jin, H.H., Lee, C.H., Lee, W.K., Lee, J.K., Park, H.C. and Yoon, S.Y. (2008), "In-situ formation of the hydroxyapatite/chitosan-alginate composite scaffolds", *Mater. Lett.*, **62**(10), 1630-1633.

Kumar, G.S., Thamizhavel, A., Yokogawa, Y., Kalkura, S.N. and Girija, E.K. (2012), "Synthesis, characterization and in vitro studies of zinc and carbonate co-substituted nano-hydroxyapatite for biomedical applications", *Mater. Chem. Phys.*, **134**(2), 1127-1135.

Lu, L. and Mikos, A.G. (1996), "The importance of new processing techniques in tissue engineering", *Mrs. Bull.*, **21**(11), 28-32.

Ma, M.G., Zhu, Y.J. and Chang, J. (2006), "Monetite formed in mixed solvents of water and ethylene glycol and its transformation to hydroxyapatite", *J. Phys. Chem. B*, **110**(29), 14226-14230.

Maguire, J.K., Cosca, M.F. and Lynch, M.H. (1987), "Problems in implantation", *Clin. Orthop.*, **216**, 213-223.

Maquet, V. and Jerome, R. (1997), "Design of macroporous biodegradable polymer scaffolds for cell transplantation", *Mater. Sci. Forum*, **250**, 15-42.

Miyaji, F., Kono, Y. and Suyama, Y. (2005), "Formation and structure of zinc-substituted calcium hydroxyapatite", *Mater. Res. Bull.*, **40**(2), 209-220.

Mourinõ, V. and Boccaccini, A.R. (2010), "Review: Bone tissue engineering therapeutics: controlled drug delivery in three-dimensional scaffolds", *J. Royal Soc. Interface*, **7**, 209-227.

Ninan, N., Muthiah, M., Park, I.K., Elain, A., Thomas, S. and Grohens, Y. (2013), "Pectin/carboxymethyl cellulose/microfibrillated cellulose composite scaffolds for tissue engineering", *Carbohyd. Polym.*, **98**(1), 877-885.

Ren, F., Xin, R., Ge, X. and Leng, Y. (2009), "Characterization and structural analysis of zinc-substituted hydroxyapatites", *Acta Biomater.*, **5**(8), 3141-3149.

Rho, J.Y., Kuhn-Spearing, L. and Zioupos, P. (1998), "Mechanical properties and the hierarchical structure of bone", *Med. Eng. Phys.*, **20**(2), 92-102.

Ribeiro, C.C., Barrias, C.C. and Barbosa, M.A. (2004), "Calcium phosphate-alginate microspheres as enzyme delivery matrices", *Biomater.*, **25**(18), 4363-4373.

Segal, L.G.J.M.A., Creely, J.J., Martin, A.E. and Conrad, C.M. (1959), "An empirical method for estimating the degree of crystallinity of native cellulose using the X-ray diffractometer", *Textile Res. J.*, **29**(10), 786-794.

Sowjanya, J.A., Singh, J., Mohita, T., Sarvanan, S., Moorthi, A., Srinivasan, N. and Selvamurugan, N. (2013), "Biocomposite scaffolds containing chitosan/alginate/nano-silica for bone tissue engineering", *Coll. Surf. B: Biointerf.*, **109**, 294-300.

Sutha, S., Karunakaran, G. and Rajendran, V. (2013), "Enhancement of antimicrobial and long-term biostability of the zinc-incorporated hydroxyapatite coated 316L stainless steel implant for biomedical application", *Ceram. Int.*, **39**(5), 5205-5212.

Tateishi, T., Chen, G., Ushida, T., Murata, T., Mizuno, S., Lewandrowski, K.U., Wise, D., Trantolo, D., Gresser, J., Yaszemski, M. and Altobelli, D. (2002), *Tissue Engineering and Biodegradable Equivalents-Scientific and Clinical Applications*, Marcel Dekker Inc., New York.

Tin-Oo, M.M., Gopalakrishnan, V., Samsuddin, A.R., Al Salihi, K.A. and Shamsuria, O. (2007), "Antibacterial property of locally produced hydroxyapatite", *Arch. Orofacial Sci.*, **2**, 41-44.

Whang, K., Tsai, D.C., Nam, E.K., Aitken, M., Sprague, S.M., Patel, P.K. and Healy, K.E. (1998), "Ectopic bone formation via rhBMP-2 delivery from porous bioabsorbable polymer scaffolds", *J. Biomed. Mater. Res.*, **42**, 491-499.

Xia, Z., Yu, X., Jiang, X., Brody, H.D., Rowe, D.W. and Wei, M. (2013), "Fabrication and characterization of biomimetic collagen–apatite scaffolds with tunable structures for bone tissue engineering", *Acta Biomater.*, **9**(7), 7308-7319.

Xiao, X., Liu, R., Chen, C. and Huang, L. (2008), "Structural characterization of zinc-substituted hydroxyapatite prepared by hydrothermal method", *J. Mater. Sci.*: *Mater. Medicine*, **19**(2), 797-803.

Xu, F.L., Li, Y.B., Han, J. and Lv, G.Y. (2005), "Biodegradable porous nano-hydroxyapatite/alginate scaffold", *Mater. Sci. Forum*, **486,** 189-192.

Zhang, S.M., Cui, F.Z., Liao, S.S., Zhu, Y. and Han, L. (2003), "Synthesis and biocompatibility of porous nano-hydroxyapatite/collagen/alginate composite", *J.Mater. Sci*: *Mater. Med.*, **14**(7), 641-645.

CC